Electro-chemo-mechanical Studies of Perovskite-Structured Mixed Ionic-Electronic Conducting $SrSn_{1-x}Fe_xO_{3-x/2+\delta}$ Part III: Thermal and Chemical Expansion

Chang Sub Kim[1], Nicola H. Perry[1,3,4], *Sean R. Bishop[1,2.3], Harry L. Tuller[1,2,3]
[1]Department of Materials Science and Engineering
Massachusetts Institute of Technology
Cambridge, MA 02139, USA
[2]Materials Research Laboratory
Massachusetts Institute of Technology
Cambridge, MA 02139, USA
[3]International Institute for Carbon-Neutral Energy Research (WPI-I[2]CNER)
Kyushu University
Fukuoka 819-0395, Japan
[4]Department of Materials Science and Engineering and Materials Research Laboratory
University of Illinois at Urbana-Champaign
Urbana IL 61801, USA

ABSTRACT

The thermal and chemical expansion of a potential solid oxide fuel cell (SOFC) cathode material $SrSn_{0.65}Fe_{0.35}O_{3-0.35/2+\delta}$ (SSF35) were investigated to assess its thermo-chemo-mechanical stability at SOFC operating temperatures and to establish the correlation between defect concentrations (oxygen vacancies and electrons) and chemical expansion with the aid of the defect chemical model reported in part I of this study. Thermochemical expansion was measured as a function of temperature and oxygen partial pressure. The chemical expansion of SSF35 showed a strong correlation with changes in oxygen nonstoichiometry associated with changes in Fe valence state. Coefficients of both chemical (CCE) and thermal (CTE) expansion were calculated and found to be smaller than that of the closely related mixed conducting perovskite oxide $SrTi_{0.65}Fe_{0.35}O_{3-0.35/2+\delta}$ (STF35). The thermal expansion coefficient of SSF was found to be close to that of YSZ (most popular solid oxide electrolyte), which makes SSF35 more attractive in terms of overall thermo-chemical stability. The chemical expansion of SSF35 showed decreasing CCE with increasing temperature and decreasing CTE with increasing oxygen deficiency, both opposite to the trends observed for STF35. Distortion in symmetry from the cubic structure seems to be responsible for the smaller coefficients and increasing asymmetry with expansion seems accountable for opposite trends of CCE and CTE compared to the STF counterpart.

Introduction

In solid oxide fuel/electrolysis cells, the electrodes must simultaneously exhibit several key properties for efficient and durable operation at high temperatures: rapid oxygen surface exchange kinetics, high bulk ionic and electronic conductivity, and themo-chemo-mechanical stability in relation to other cell components. This latter property typically requires a coefficient of thermal expansion (CTE) that matches that of the electrolyte, as well as minimal chemical expansion in response to temporal or spatial oxygen concentration changes. Since superior oxygen electrodes are typically mixed conductors that readily change their level of oxygen nonstoichiometry, δ in $ABO_{3-\delta}$, with changes in pO_2 and temperature, they commonly exhibit non-negligible levels of chemical expansion. In fact, the total effective coefficient of thermal expansion at elevated temperatures, where mixed conductors not only expand thermally but also expand chemically as they lose oxygen, can be twice the value of the CTE alone (*1–3*). Phenomenologically, the chemical strain (ε_C) at a given temperature is often observed to be proportional to the change in oxygen content, and so it can be described as in equation (1):

$$\varepsilon_C = \alpha_C \Delta\delta \qquad (1)$$

* Present address: Redox Power Systems, College Park, MD 20742

In previous papers in this series (parts I and II), we introduced the mixed conductor $SrSn_{1-x}Fe_xO_{3-x/2+\delta}$ (SSF) – analogous to a well-known model oxygen electrode $SrTi_{1-x}Fe_xO_{3-x/2+\delta}$ (STF) – and examined how replacing a B-site host cation Ti^{4+} with Sn^{4+} would affect the defect chemistry and electro-ionic transport models (*4*, *5*). In part I, we showed how the oxygen content, δ, changes from the reference point (*3-x/2* as a result of doping *x* concentration of Fe^{3+} in Sn^{4+} site) as a function of temperature and oxygen partial pressure, as measured by thermogravimetric analysis (TGA) (*4*). In part II, we observed its related mixed conductivity behavior and noted that its oxygen surface exchange kinetics were as rapid as those of the well-known model oxygen electrode $SrTi_{1-x}Fe_xO_{3-x/2+\delta}$ (STF) (*5*). In the present contribution we turn to understanding the thermo-chemical expansion behavior in comparison to that of the previously characterized STF (*6*). Chemical expansion upon oxygen loss in STF has been attributed primarily to enlargement of the multivalent Fe cations as they gain electrons (*6*). On average, in perovskites, oxygen vacancies appear to have a similar or slightly smaller effective ionic radius to that of the oxide ion, so their generation is not thought responsible for the expansion (*7*). The magnitude of lattice expansion in this case may depend on the extent of electron localization on the multivalent cation (as has been shown for both STF (*6*) and other mixed conducting perovskites) (*8*), as well as the average valence state of that cation (e.g., 4+ → 3+ transitions vs. 3+ → 2+ transitions), since these factors both affect the magnitude of change in the Fe ionic radius (*9*). Within perovskites more generally, factors found to influence the magnitude of the CCE include: size of the anion vacancy, extent of charge localization on multivalent cations, crystal symmetry, and temperature (*10–13*). In comparison to STF, SSF is expected to demonstrate a similar CCE under oxidizing conditions, owing to the key role of multivalent Fe in both systems, and similar hole mobilities (*5*) (i.e., presumably similar charge localization on Fe under oxidizing conditions). (Under reducing conditions the CCE may differ, owing to differences in measured electron mobilities and therefore possibly changes in the extent of charge localization on Fe in these conditions.) On the other hand, owing to the larger size of Sn^{4+} (0.69 Å, VI-fold coordination) vs. Ti^{4+} (0.605 Å, VI-fold coordination) (*9*) occupying the perovskite B sites shared by Fe, SSF exhibits a slight orthorhombic distortion (vs. cubic STF), a larger unit cell, and possibly a greater tendency to order (given Sn and Fe size mismatch), which could all impact the CCE via the aforementioned factors, impact the CTE, and ultimately lead to changes in thermo-chemo-mechanical stability relative to STF.

In the present work we measure the CTE in air and determine the isothermal CCE at various temperatures for $SrSn_{0.65}Fe_{0.35}O_{3-0.35/2+\delta}$ (SSF35) using dilatometric measurements of macroscopic chemical strain obtained in this study combined with the previously measured oxygen content changes by TGA (*4*). In addition, using new TGA measurements of SSF35 oxygen stoichiometry to lower temperatures and the measured CTE and CCE, the full thermo-chemical expansion upon heating in air is modeled, in a similar analysis to our previous work on STF35 (*6*). Finally, we also provide *in situ* X-ray diffraction analysis of thermo-chemical expansion in different gas atmospheres to provide a crystal-structure-level view complementing the macroscopic analysis. The results show that SSF35 exhibits lower CTEs and CCEs compared to STF35, and therefore, in combination with its rapid oxygen surface exchange kinetics and mixed conductivity, represents a promising alternative oxygen electrode material with better thermo-chemo-mechanical stability.

Experimental

SSF solid solutions were prepared by ball milling assisted solid state reaction, the same method as used in the previous studies, parts I and II (*4*, *5*). Rectangular bar-shaped SSF bulk samples were prepared with dimensions of 21×2.7×2.47 mm^3 for both chemical expansion and thermogravimetric studies. The prepared powders were placed in a rectangular bar-shaped stainless steel die, uniaxially pressed at 20 MPa for two minutes, and then sintered for six hours in air at 1500 °C with heating and cooling at 5 °C/min. The relative density of the bulk samples measured through Archimedes' principle was approximately 97%. Thermal and chemical expansions were measured by a Linseis L75 PT Horizontal

Dilatometer (Robbinsville, NJ) with quartz sample holder and push-rod. Thermogravimetry was performed with the Cahn Model 2000 Electrobalance used in part I of the study (*4*). For controlled gas environments, 1000 ppm oxygen and ultra high purity oxygen and nitrogen tanks were used, controlled by MKS mass flow controllers. A cylindrical bulk sample of 1-inch diameter was prepared for high temperature XRD measurements using a PANalytical X'pert Pro diffractometer (Westborough, MA). The XRD sample was measured at 100 °C decrements from 900 °C to 500 °C (in air) and 600 °C (in 1000 ppm O_2), then at room temperature after one hour of holding time to make sure the sample was in equilibrium (at elevated temperatures). Samples were scanned using Cu Kα radiation over the 2θ range 20-100° with a step size of 0.008° and a scan speed of 1.6°/min. XRD patterns were fitted using Rietveld refinement, allowing refinement of specimen displacement but not goniometer zero offset, with Highscore Plus software.

Results and discussion

Thermo-chemical expansion in air

The thermo-chemical expansion of SSF35 was measured by dilatometry in air as a function of temperature, during cooling at 2 °C min^{-1} as well as at steady-state, referenced to the final room temperature values, as shown in Figure 1. For comparison, STF counterpart (STF35) expansions during cooling and at steady-states from Perry et al. are also plotted (*6*).

Total expansion (ε_{TOT}) is the sum of both thermal (ε_T) and chemical (ε_C) expansions. Chemical expansion under reduction results, as described above, from the net effect of oxygen vacancy generation and the localization of surplus electrons at the metal cations (*7*). In the low temperature regime (≤ 500 °C), both oxygen surface exchange and bulk diffusion slows down significantly so that the oxygen vacancy concentration is frozen in and the effect of chemical expansion becomes negligible, thereby only exhibiting linear thermal expansion. In the high temperature regime (> 500 °C), because the expansion comes from both thermal and chemical effects, the slope is steeper compared to the low temperature regime. Moreover, in this high temperature regime, there is a difference in strain between steady state and non-equilibrium states (during cooling) as expansion/contraction is limited by oxygen surface exchange and/or oxygen vacancy diffusion in bulk.

The coefficient of thermal expansion (CTE) of SSF35 was measured to be 10.22 ppm per °C at lower temperatures. The CTE of the STF counterpart during cooling was reported to be 12.3 ppm per °C (*6*). The lower CTE of SSF is likely due to the asymmetric nature of the SSF crystal structure (orthorhombic, close to tetragonal) confirmed by XRD in part 1 of the paper compared to the cubic STF (*4*). The CTE of SSF35 is surprisingly close to that of the most commonly used electrolyte material for SOFC – 8YSZ, which has a CTE of 10.5 ppm per °C (*14*). Therefore, with similar surface exchange kinetics (*4*), SSF35 is viewed as a superior choice given its better chemo-mechanical compatibility with YSZ.

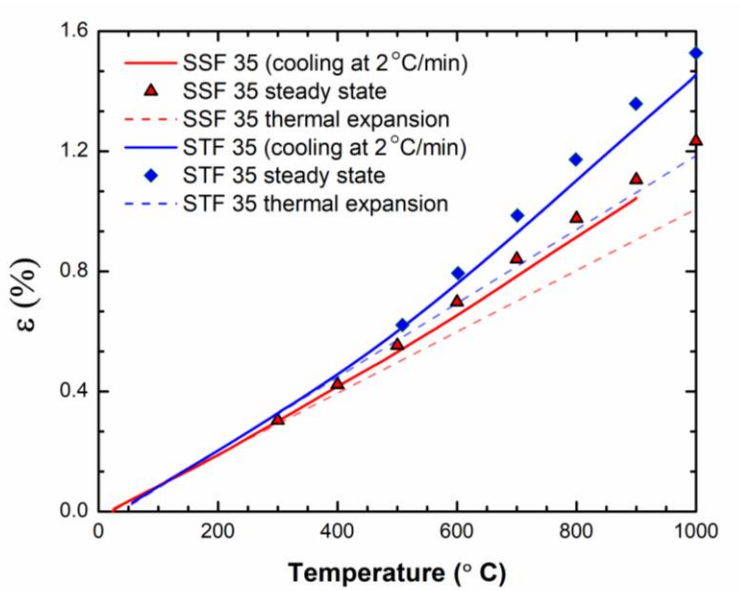

Figure 1. Measured strain of SSF35 in air during cooling at 2 °C per minute (red line) and at equilibrium states (red triangles). Expansion of STF35 by Perry et al. is plotted in blue for comparison (*6*)**. Thermal expansions extended from low temperature regime (below 200 °C) are plotted in red (SSF) and blue (STF) dashed lines.**

Theoretical calculation of oxygen nonstoichiometry, δ, based upon the defect model derived in Part I of this series and measurements of the bar-shaped bulk taken during cooling at 2 °/min are shown in Figure 2. The oxygen nonstoichiometry is frozen in below 500 °C, agreeing with the expansion measurements above. The slight decrease in δ below 400 °C is likely due to a buoyancy effect (vertical tube with both ends open) during measurement.

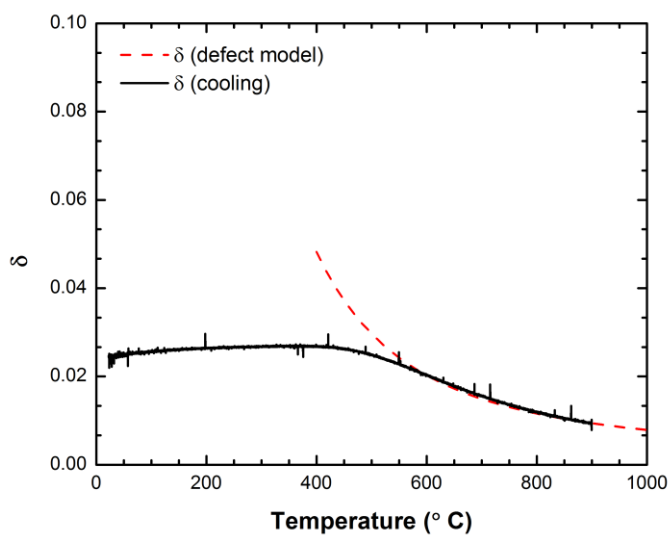

Figure 2. Oxygen nonstoichiometry, δ, as a function of temperature for $SrSn_{0.65}Fe_{0.35}O_{2.825+\delta}$ (SSF35) calculated from the defect model (dashed line) and measured during cooling in air from 900 °C at 2 °C min^{-1} using thermogravimetry.

Isothermal chemical expansion

The total expansion of SSF can be deconvoluted as:

$$d\varepsilon_{\mathrm{TOT}} = \left(\frac{\partial \varepsilon}{\partial T}\right)_{\delta} \mathrm{d}T + \left(\frac{\partial \varepsilon}{\partial \delta}\right)_{T} \mathrm{d}\delta = \alpha_{\mathrm{T}} \mathrm{d}T + \alpha_{\mathrm{C}} \mathrm{d}\delta \qquad (2)$$

where α_{T} is the iso-stoichiometric CTE and α_{C} is the isothermal CCE *(6)*. In order to systematically study isothermal chemical expansion, dilation of SSF35 was measured as a function of oxygen partial pressure in four different isotherms between 700 and 1000 °C. As an example, isothermal chemical expansion measurements at 700 °C are shown in Figure 3 as a function of pO_2 achieved by controlling the oxygen/nitrogen gas mixture ratio over time. The expansion values are referenced to the sample length at room temperature.

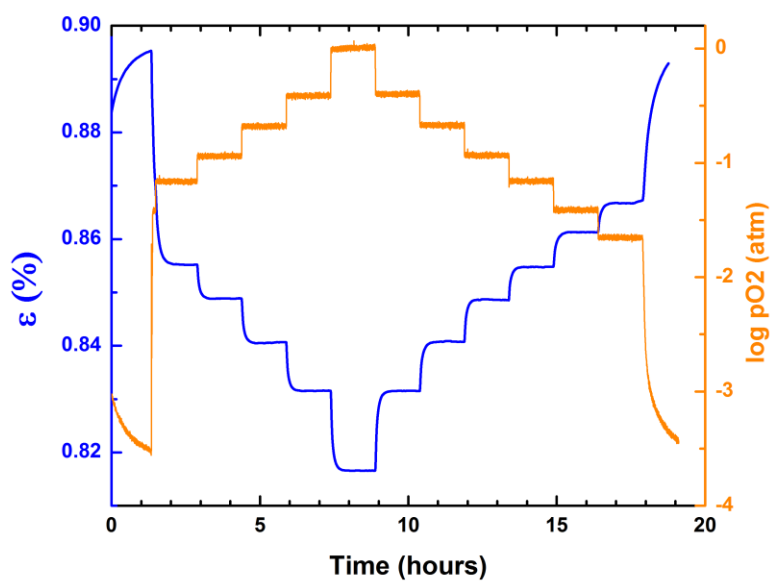

Figure 3. Plot of isothermal chemical expansion and pO_2 over time at 700 °C. The expansion values are referenced to the sample at room temperature.

The chemical expansion of SSF35 is observed to be reversible upon periodic oxidation and reduction steps in the SSF bulk sample. One does however observe relaxations in strain upon the imposition of step changes in pO_2 that are related to a combination of oxygen surface exchange kinetics and diffusion of oxygen vacancies within the bulk needed to achieve the next stage of equilibrium.

The chemical expansion of SSF35 is plotted in a series of four isotherms in Figure 4. Strain is referenced to the dimensions at room temperature in air, and the oxygen non-stoichiometry, δ, at a given temperature and oxygen partial pressure, was determined from thermogravimetric analysis as described in part I of this study (*4*).

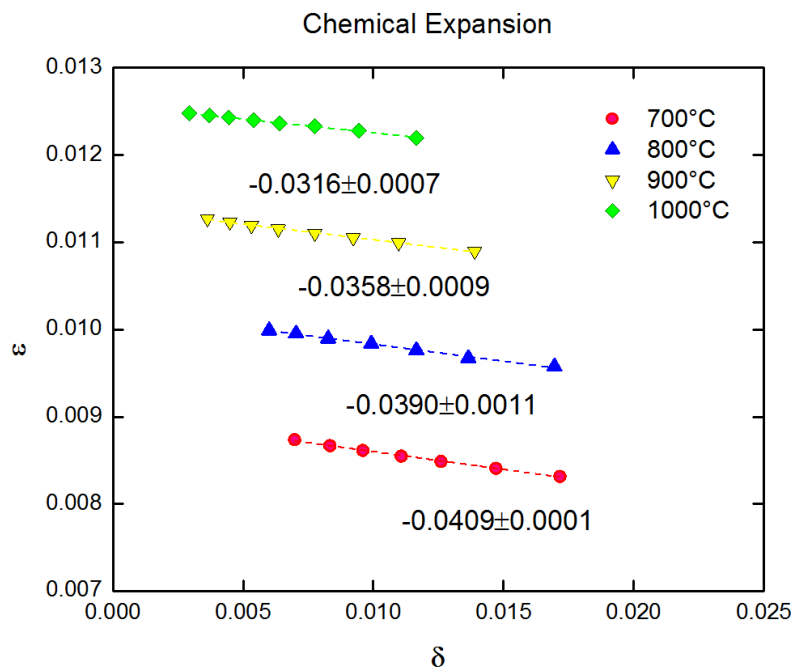

Figure 4. Expansion of SSF35 (relative to a reference point at 27 °C, 0.21 atm pO_2) as a function of oxygen non-stoichiometry at four isotherms (700~1000 °C). The values for the slopes together with their uncertainties are indicated, with the magnitudes corresponding to the coefficients of chemical expansion.

The linear dependence of isothermal expansion on oxygen non-stoichiometry in Figure 4 enables fitting of the data to calculate expansion coefficients corresponding to a particular value of non-stoichiometry at each temperature. The magnitude of such slope is defined as an isothermal CCE (α_C), since lower δ corresponds to higher number of oxygen vacancies. The CCE of SSF35 decreases as temperature increases, unlike CCE of STF35 which has positive temperature dependence (*6*). Again, this could be due to the asymmetric crystal structure of SSF – close-to-tetragonal – and an increase in asymmetry with temperature. Since the CCE of SSF35 is lower than that of STF35 at high temperatures (>700 °C, SOFC operating temperatures), SSF35 would be more suitable for actual SOFC implementation.

The dependence of isothermal CCE (α_C) on temperature (in °C) in this high temperature range, which is to a first approximation linear ($R^2 = 0.0985$), can be expressed as (*6*):

$$\alpha_C = -2.950 \times 10^{-5}\, T + 6.156 \times 10^{-2} \qquad (3)$$

Iso-stoichiometric thermal expansion

Interpolating and extrapolating each isothermal CCE from Figure 4, iso-stoichiometric expansion of SSF35 can be calculated and plotted in Figure 5.

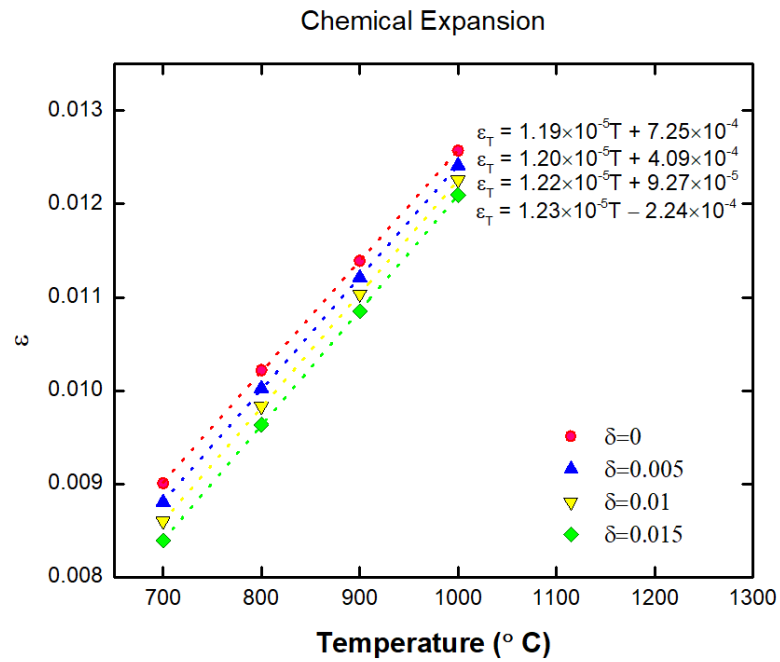

Figure 5. Iso-stoichiometric expansion of SSF35 vs. temperature for δ=0, 0.005, 0.01, and 0.015, interpolated/extrapolated from Figure 4.

The four iso-stoichiometric thermal expansion curves show a linear dependence on temperature, with the linear equations relating ε and T included in Figure 5. The slopes represent iso-stoichiometric coefficients of thermal expansion (CTEs), which linearly depend on the oxygen non-stoichiometry δ and can be expressed as:

$$\alpha_T = 3.105 \times 10^{-5}\,\delta + 1.185 \times 10^{-5} \qquad (4)$$

This CTE dependency on δ for SSF35 (increasing CTE with δ) is opposite of what Perry, et al observed for STF35 (decreasing CTE with δ) (*6*). This trend is consistent with the earlier observation of decreasing CCE with T.

In-situ X-ray diffraction

In order to study thermo-chemical expansion of the SSF35 lattice directly, high-temperature in-situ XRD was performed in two different atmospheres – in air and 1000 ppm of oxygen. The XRD peaks corresponded to orthorhombic Pbnm space group, which was used in the Rietveld refinement to determine lattice parameters (a, b, and c), as shown in Figure 6. Pseudo-cubic lattice constants were also determined using the formulas $a_{pc} = \frac{a \text{ or } c}{\sqrt{2}} = \frac{b}{2}$. Pseudo-cubic parameters were averaged at each temperature and compared with the expansion values from dilatometry in Figure 7. The pseudo-cubic parameters show the same thermo-chemical behavior as expansion measured by dilatometry under steady-state conditions. Expansion values in air, using the two different means, agree well with each other. The effect of chemical expansion is also evident from the pseudo-cubic parameter values, and the trend (decrease in chemical expansion with temperature) confirms the differences of thermo-chemical behavior between SSF35 and STF35.

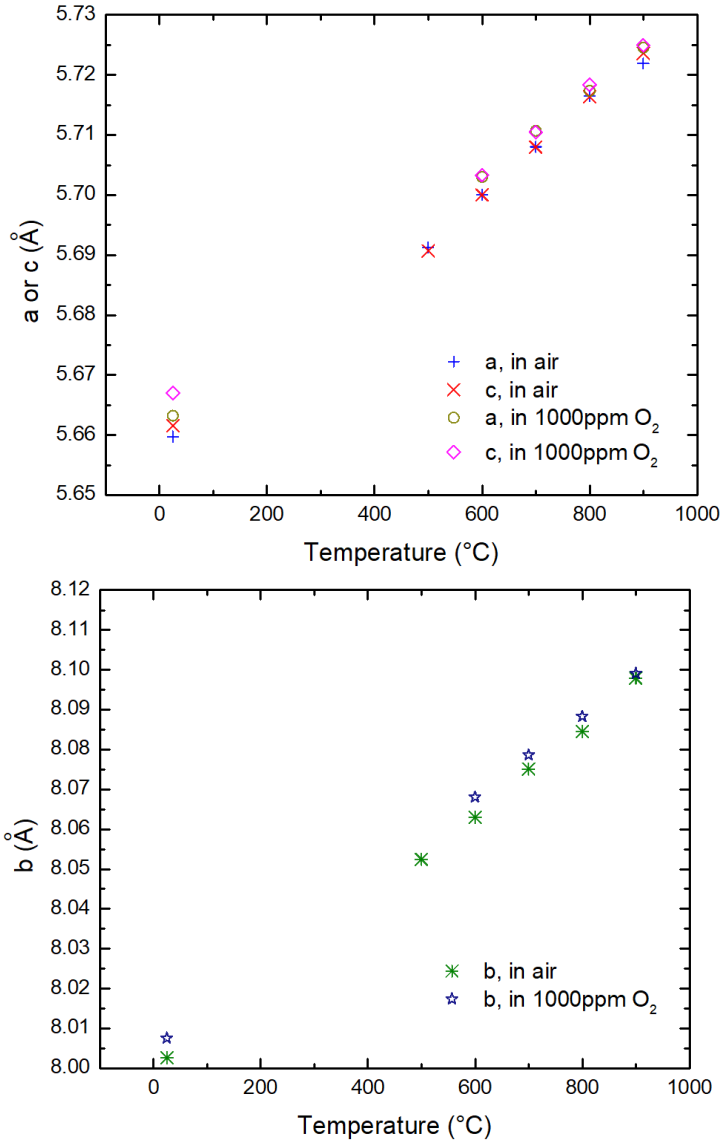

Figure 6. Lattice parameters (a, b, and c) of SSF35 in room temperature and high temperatures derived from *in-situ* high temperature XRD in air and in 1000 ppm of oxygen.

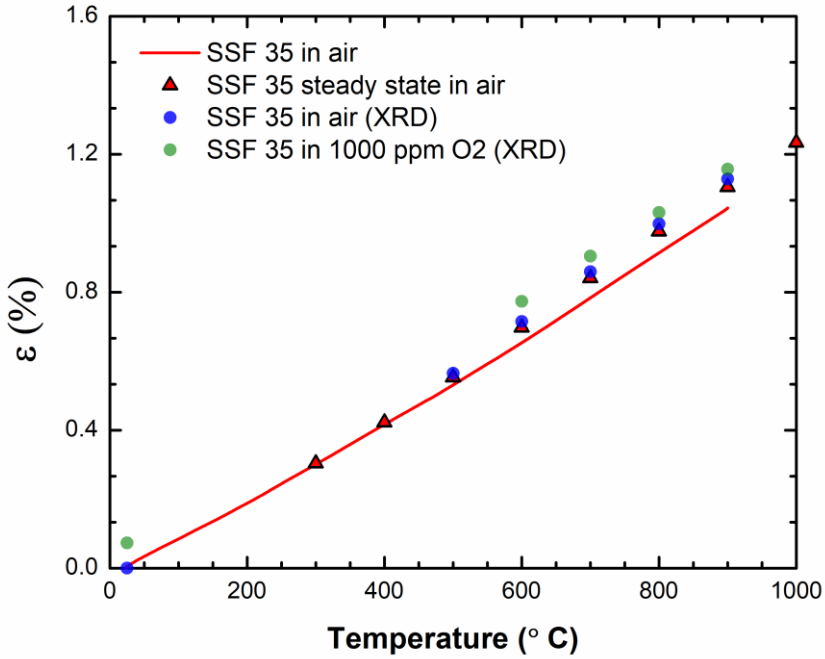

Figure 7. Expansion of SSF 35 from dilatometry while cooling at 2 °/min in air (red line) and at steady state (red triangles), and from average lattice parameters of pseudo-cubic fitting from XRD in air (orange squares) and in 1000 ppm O_2 (magenta squares).

Comparison of thermo-chemical properties of SSF35 and STF35 is summarized in Table 1 below.

Table 1.

	SSF35	**STF35**
α_C	$-2.950 \times 10^{-5}\, T + 6.156 \times 10^{-2}$	$3.0(3) \times 10^{-5}\, T + 1.9(2) \times 10^{-2}$
α_C at 800 °C	0.039	0.0431
α_T (per °C)	$3.105 \times 10^{-5}\, \delta + 1.185 \times 10^{-5}$	$-3.00 \times 10^{-5}\, \delta + 1.44 \times 10^{-5}$
α_T below 500 °C	$10.22 \cdot 10^{-6}$/ °C	$12.3 \cdot 10^{-6}$/ °C

CONCLUSIONS

Thermochemical expansion of a promising SOFC cathode material $SrSn_{0.65}Fe_{0.35}O_{3-0.35/2+\delta}$ (SSF35) was measured and analyzed using the defect chemical model derived from part I of this study. Coefficients of both chemical and thermal expansion were extracted, and expressions for their temperature and oxygen non-stoichiometry dependence were derived. The coefficient of thermal expansion of SSF35 was 10.22 ppm per °C, smaller than that of STF35 and close to that of YSZ, the predominant solid electrolyte used in SOFC applications. At high temperatures, the CTE increased with δ (or decreased with increasing oxygen nonstoichiometry from O_3), a trend opposite to that of STF35. The coefficient of chemical

expansion for SSF35 is also smaller than that of its STF counterpart and with opposite trend of temperature dependence. This behavior is, we believe, due to the asymmetry in SSF35's crystal structure – close-to-tetragonal – compared to close-to-cubic structure of STF35. Expansion was also measured by *in-situ* XRD at high temperatures in air and in 1000 ppm of oxygen. SSF35 showed pseudo-cubic structures at high temperatures, and the fitted lattice strain agreed well with the macroscopic measurements using dilatometry. Considering the comparable surface oxygen exchange kinetics to that exhibited by its STF counterpart, as reported in part II of this study (*5*), excellent CTE match with 8YSZ, and smaller CCE compared to the STF35, SSF35 would appear to be an excellent alternate choice to serve as a SOFC cathode material.

Acknowledgments

This research was carried out as a part of the activity of the Skoltech-MIT Center for Electrochemical Energy Storage. Structural characterization of the materials was conducted in the MRSEC Shared Experimental Facilities at MIT, supported by the National Science Foundation under award number DMR-1419807. Thanks go to Dr. Charlie Settens for assistance with XRD.

REFERENCES

1. S. R. Bishop, K. L. Duncan, E. D. Wachsman, Thermo-chemical expansion in strontium-doped lanthanum cobalt iron oxide. *J. Am. Ceram. Soc.* **93**, 4115–4121 (2010).
2. S. B. Adler, Chemical Expansivity of Electrochemical Ceramics. *J. Am. Ceram. Soc.* **84**, 2117–2119 (2001).
3. S. R. Bishop *et al.*, Chemical Expansion: Implications for Electrochemical Energy Storage and Conversion Devices. *Annu. Rev. Mater. Res.* **44**, 205–239 (2014).
4. C. S. Kim, S. R. Bishop, N. H. Perry, H. L. Tuller, Electro-chemo-mechanical studies of perovskite-structured mixed ionic-electronic conducting $SrSn_{1-x}Fe_xO_{3-x/2+\delta}$part I: Defect chemistry. *J. Electroceramics*. **38**, 74–80 (2017).
5. C. S. Kim, S. R. Bishop, H. L. Tuller, Electro-chemo-mechanical studies of perovskite-structured mixed ionic-electronic conducting $SrSn_{1-x}Fe_xO_{3-x/2+\delta}$ part II: Electrical conductivity and cathode performance. *J. Electroceramics*, 1–8 (2017).
6. N. H. Perry, J. J. Kim, S. R. Bishop, H. L. Tuller, Strongly coupled thermal and chemical expansion in the perovskite oxide system $Sr(Ti,Fe)O_{3-a}$. *J. Mater. Chem. A.* **3**, 3602–3611 (2015).
7. D. Marrocchelli, N. Perry, S. Bishop, Understanding chemical expansion in perovskite-structured oxides. *Phys. Chem. Chem. Phys.* **17**, 10028–10039 (2015).
8. N. H. Perry, J. E. Thomas, D. Marrocchelli, S. R. Bishop, H. L. Tuller, Isolating the Role of Charge Localization in Chemical Expansion: $(La,Sr)(Ga,Ni)O_{3-x}$ Case Study. *ECS Trans.* **57**, 1879–1884 (2013).
9. R. D. Shannon, Revised effective ionic radii and systematic studies of interatomic distances in halides and chalcogenides. *Acta Crystallogr. Sect. A.* **32**, 751–767 (1976).

10. X. Chen, J. Yu, S. B. Adler, Thermal and chemical expansion of Sr-doped lanthanum cobalt oxide ($La_{1-x}Sr_xCoO_{3-\delta}$). *Chem. Mater.* **17**, 4537–4546 (2005).

11. N. H. Perry, D. Marrocchelli, S. R. Bishop, H. L. Tuller, (Invited) Understanding and Controlling Chemo-Mechanical Coupling in Perovskite Oxides. *ECS Trans.* **72**, 1–8 (2016).

12. V. V. Kharton, A. a. Yaremchenko, M. V. Patrakeev, E. N. Naumovich, F. M. B. Marques, Thermal and chemical induced expansion of $La_{0.3}Sr_{0.7}(Fe,Ga)O_{3-\delta}$ ceramics. *J. Eur. Ceram. Soc.* **23**, 1417–1426 (2003).

13. S. McIntosh, J. F. Vente, W. G. Haije, D. H. A. Blank, H. J. M. Bouwmeester, Oxygen stoichiometry and chemical expansion of $Ba_{0.5}Sr_{0.5}Co_{0.8}Fe_4O_{3-\delta}$- measured by in situ neutron diffraction. *Chem. Mater.* **18**, 2187–2193 (2006).

14. I. Yasuda, M. Hishinuma, Lattice expansion of acceptor-doped lanthanum chromites under high-temperature reducing atmospheres. *Electrochemistry*. **68**, 526 (2000).